Received: 29 September 2019 | Revised: 20 January 2020 | Accepted: 20 January 2020

DOI: 10.1002/jccs.201900365

JOURNAL OF THE CHINESE CHEMICAL SOCIETY

ARTICLE

Ultrasound-assisted synthesis of 3-(1-(2-(1*H*-indol-3-yl) ethyl)-2-aryl-6,6-dimethyl-4-oxo-4,5,6,7-tetrahydro-1*H*-indol-3-yl)indolin-2-ones by novel core-shell bio-based nanocatalyst anchoring sulfonated *L*-histidine on magnetized silica (SO_3H-*L*-His@SiO_2-nano Fe_3O_4)

Kobra Nikoofar | **Seyedeh S. Peyrovebaghi**

Department of Chemistry, Faculty of Physics and Chemistry, Alzahra University, Tehran, Iran

Correspondence
Kobra Nikoofar, Department of Chemistry, Faculty of Physics and Chemistry, Alzahra University, Tehran, Iran.
Email: k.nikoofar@alzahra.ac.ir, kobranikoofar@yahoo.com

Funding information
Alzahra University

Abstract

An efficient synthesis of 3-(1-(2-(1*H*-indol-3-yl)ethyl)-2-aryl-6,6-dimethyl-4-oxo-4,5,6,7-tetrahydro-1*H*-indol-3-yl)indolin-2-ones is reported via a one-pot three-component reaction of 3-phenacylidenoxindoles, tryptamine, and dimedone under ultrasound irradiation using a newly prepared core-shell nanostructure. The utilized nanocatalyst is obtained by anchoring sulfonated *L*-histidine amino acid shell, as the bio part, on silica-nanomagnetite core (SO_3H-*L*-His@SiO_2-nano Fe_3O_4) and characterized by Fourier transform infrared spectroscopy, nuclear magnetic resonance spectroscopy (^{1}H NMR), field emission scanning electron microscopy, energy-dispersive X-ray spectroscopy, thermogravimetric/differential thermal analysis, vibrating sample magnetometer measurements, transmission electron microscopy, and back-titration. The protocol contains several advantages, such as relatively short reaction times, simple work-up procedure by separation of the catalyst with an external magnet, the use of economical and environmentally friendly ultrasonic waves, and reusability and recoverability of the core-shell nano-promoter for three runs without significant activity loss.

KEYWORDS

3-phenacylidenox, indole, core-shell nanostructure, indole, nanomagnetite, tetrahydro-1*H*-indolyl-indolin-2-ones, tryptamine, ultrasound irradiation

1 | INTRODUCTION

Indoline-2-one (2-oxindole), a bicyclic compound made up of a fused benzene to 2-pyrrolidone, is a versatile heterocycle which is also a building block in various kinds of organics and pharmaceuticals.[1] Semaxanib (Figure 1a) as tyrosine kinase inhibitor[2] and SM-130686 (Figure 1b) as a growth hormone secretagogue receptor agonist[3] are two examples of potent drugs containing the indoline-2-one scaffold.

The indoline-2-one motif is associated in some compounds with various properties such as anti-angiogenic and antitumor,[4,5] antibacterial and antifungal,[6] antiplasmodial,[7] and anti-human immunodeficiency

© 2020 The Chemical Society Located in Taipei & Wiley-VCH Verlag GmbH & Co. KGaA, Weinheim

virus.[8] Because of the critical importance of 2-indlolinone motif in organic heterocycles with proven and/or potent therapeutic properties, methods for their synthesis have been of great interest since the last decade.[9–13]

Sonochemistry, which is the study of the effects of ultrasound on chemical reactions, has been recognized as an efficient strategy for a vast range of organic transformations as a green and economical technique. Because of its specific characteristics, it could assist in high-energy chemical reactions in shorter periods in comparison to traditional methods. Actually, when the reaction mixture is exposed to sonic waves, they generate high microscopic pressure, due to cavity and hot-spot effects, which increases the energy in seconds and leads to the acceleration of the reaction.[14–16] Nowadays it is also an operational technique to obtain nano-sized materials.[17,18]

Magnetic nanoparticles have attracted special attention in various fields of study such as the environment,[19] biomedicine and drug delivery,[20,21] treatment monitoring,[22] magnetic resonance imaging,[23] and waste removal form water.[24] Besides, it is very important for chemists as a catalyst in various kinds of transformations, especially multicomponent reactions (MCRs).[25–29]

In continuation of our research interest in green and economical routes for the synthesis of heterocycles by novel nanostructures,[30–34] here we report the preparation of 3-(1-(2-(1*H*-indol-3-yl)ethyl)-2-aryl-6,6-dimethyl-4-oxo-4,5,6,7-tetrahydro-1*H*-indol-3-yl)indolin-2-ones via the three-component reaction of 3-phenacylideneoxindoles (**1**), tryptamine (**2**), and dimedone (**3**) in acetonitrile in the presence of a novel nano core-shell prepared from functionalized L-histidine and magnetized silica (SO_3H-L-His@SiO_2-nano Fe_3O_4) though ultrasound irradiation of power 60 W/cm^2 (Scheme 1). It is noteworthy that Jiang and Yan in 2016 obtained some derivatives of this class of N-containing multi-cycles in the presence of *p*-TsOH within 6 h in 72–87% yield.[35]

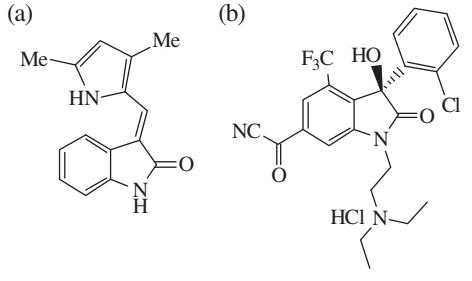

FIGURE 1 (a) Semaxanib and (b) SM-130686

2 | RESULTS AND DISCUSSION

In this study, a novel functionalized core-shell multilayered nanostructure was prepared by anchoring sulfonated histidine on magnetized silica (SO_3H-*L*-His@SiO_2-nano Fe_3O_4). The four-step schematic procedure is illustrated in Scheme 2.

The Fourier transform infrared (FT-IR) spectra of final nanostructures, in addition to those at each step, are shown in Figure 2. As seen from Figure 2a, the stretching vibrations of the Fe–O bond at 1646 and 1455 cm^{-1} and the bending vibration of this bond at 575 cm^{-1} are the fingerprints of commercial Fe_3O_4. The spectrum of *L*-histidine (Figure 2b) shows a broad peak at 2708–3124 cm^{-1}, which is due to the stretching vibration of the NH_3^+ group and bending vibrations of the N–H bond at 1591 and 804 cm^{-1}. The asymmetric and symmetric stretching of the COO^- group at 1635 and 1340 cm^{-1}, in addition to the peaks at 1461, 1416, and 1249 cm^{-1} corresponding to the C=C, C=N, and C–N bonds, respectively, confirmed the histidine structure. The SiO_2-nano Fe_3O_4 spectra in Figure 1c contain the magnetic nanoparticles peaks in addition to the bands corresponding to the stretching vibration of the OH group in silanol at 3419 cm^{-1}, the stretching of the Si–O–H bond at 1121 cm^{-1}, and the stretching of the Si–O–Si bond at 1214 cm^{-1}. Anchoring of *L*-histidine to this core led to the appearance of the amino acid peaks (Figure 1d). The FT-IR spectra of the SO_3H-*L*-His@SiO_2-nano Fe_3O_4 (Figure 2e) show peaks at 1260, 1085, and

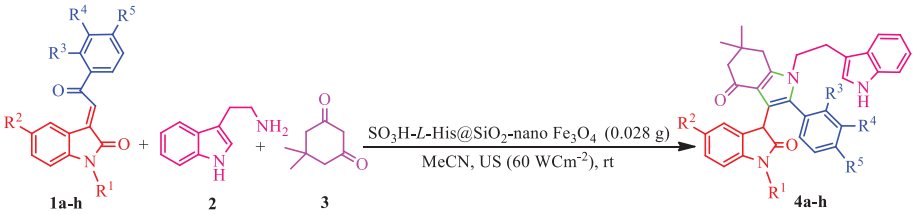

R^1 = H, CH_2Ph
R^2 = H, Cl
R^3 = H, OH, Br
R^4 = H, OMe
R^5 = H, OMe, OH, NO_2

SCHEME 1 Preparation of 3-(1-(2-(1*H*-indol-3-yl)ethyl)-2-aryl-6,6-dimethyl-4-oxo-4,5,6,7-tetrahydro-1*H*-indol-3-yl)indolin-2-ones

SCHEME 2 Synthetic procedure of SO_3H-*L*-His@SiO_2-nano Fe_3O_4

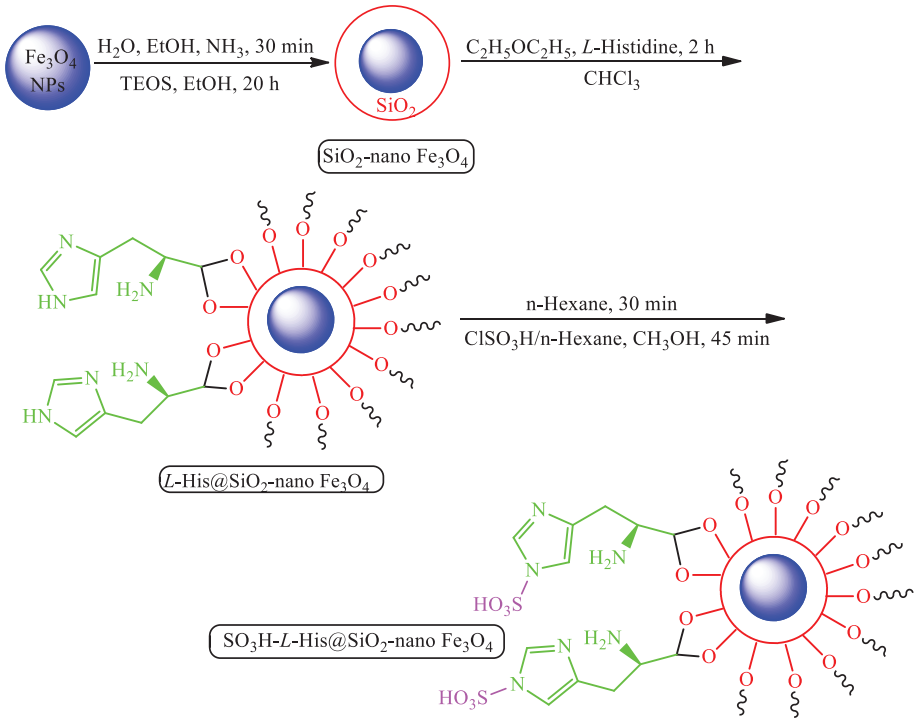

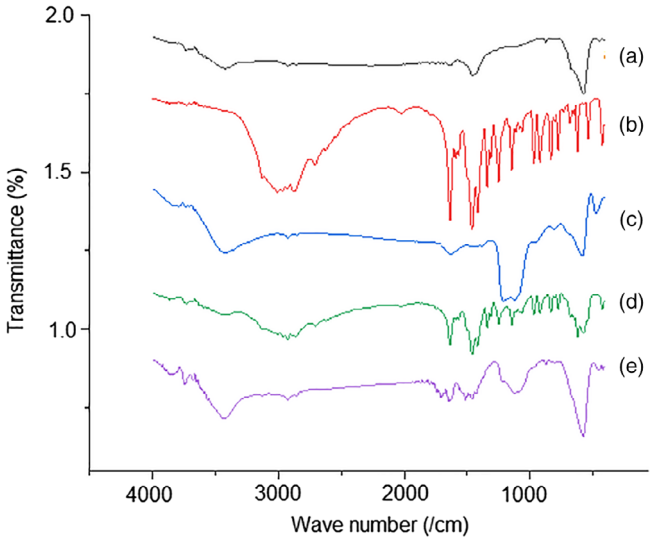

FIGURE 2 FT-IR spectra of (a) nano Fe_3O_4, (b) *L*-Histidine, (c) SiO_2-nano Fe_3O_4, (d) *L*-His@SiO_2-nano Fe_3O_4, and (e) SO_3H-*L*-His@SiO_2-nano Fe_3O_4

873 cm^{-1} corresponding to the asymmetric and symmetric stretching vibrations of S═O and stretching vibrations of the S–O bond, respectively. It must be mentioned that the band at 3423 cm^{-1}, due to the hydroxyl moiety of SO_3H, is partially covered by the stretching band of NH.

The field emission scanning electron microscopy (FESEM) images of *L*-His@SiO_2-nano Fe_3O_4 (top) and SO_3H-*L*-His@SiO_2-nano Fe_3O_4 (bottom) are shown in Figure 3. The average size of the nanoparticles in *L*-His@SiO_2-nano Fe_3O_4 is 50–70 nm and the average diameter for the final core-shell nanostructure is between 70 and 90 nm. The increased particle size confirmed the layer structure of the core due to the functionalization process.

Figure 4 presents the energy-dispersive X-ray spectroscopy (EDAX) patterns of (a) *L*-His@SiO_2-nano Fe_3O_4 and (b) SO_3H-*L*-His@SiO_2-nano Fe_3O_4. The measurement confirmed the presence of elements such as C (23.47%), N (9.34%), Si (1.46%), O (41.05%), and Fe (29.97%) in *L*-His@SiO_2-nano Fe_3O_4, proving its successful preparation. The presence of sulfur (0.16%) in the final nano core-shell confirmed its functionalization. No other impurities related to the solvents and materials used in the catalyst manufacturing process were observed.

In the transmission electron microscopy (TEM) images of SO_3H-*L*-His@SiO_2-nano Fe_3O_4 (Figure 5), the dark parts are related to the internal nucleus of the nanostructures while the lighter parts explain the outer parts (shell) of the core. The particle size correlates with that in the FESEM images.

The magnetic properties of the compound were investigated by vibrating sample magnetometer (VSM) analysis at room temperature (Figure 6). Based on the curves 1–3, the saturation magnetization values of 63, 56, and 42 emu g^{-1} are due to commercial nano-magnetite, *L*-His@SiO_2-nano Fe_3O_4, and functionalized SO_3H-*L*-His@SiO_2-nano Fe_3O_4, respectively. The decreasing value from curve 1 to curve 3 can be attributed to the layers on

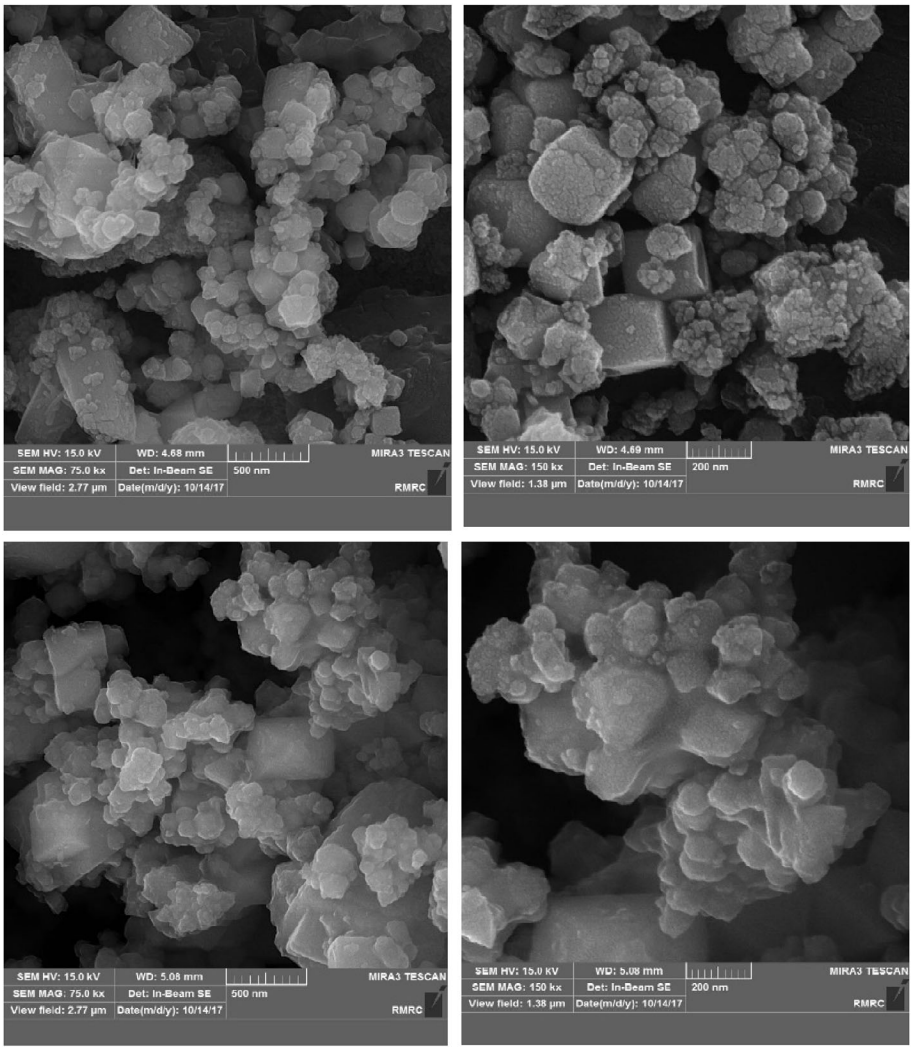

FIGURE 3 FESEM images of *L*-His@SiO_2-nano Fe_3O_4 (top) and SO_3H-*L*-His@SiO_2-nano Fe_3O_4 (bottom)

the nano Fe_3O_4 internal core. The significant superparamagnetism of the synthesized nanomaterials is sufficiently strong to offer a simple and efficient method to separate the catalyst from the reaction media by an external magnet.

Thermogravimetric/differential thermogravimetry (TG/DTG) analyses results of *L*-His@SiO_2-nano Fe_3O_4 and the final nanocatalyst SO_3H-*L*-His@SiO_2-nano Fe_3O_4 are shown in Fig. 7a and b, respectively. As can be seen from the figure, the endothermic degradation of *L*-His@SiO_2-nano Fe_3O_4 (Figure 7a) occurs in two stages. The first one occurring at 260–290°C (about 10% weight loss) is due to the degradation of the organic layer, whereas the second weight loss of about 70% at 630–700 °C is due to the total decay of the structure. In the case of SO_3H-*L*-His@SiO_2-nano Fe_3O_4 (Figure 7b), desulfonation occurs at 190–210 °C (about 5% weight loss) and total degradation occurs at 310–550 °C. These observations are in agreement with the fact that the systems are binary organic–inorganic frameworks and that the organic parts are less heat-resistant and are destroyed earlier.

The total acidity of the core-shell nanostructure (SO_3H-*L*-His@SiO_2-nano Fe_3O_4) was investigated by back-titration. First, 0.1 g of the nanocatalyst and 25 mL of NaOH (0.1 M) were mixed together and stirred for 24 h on a magnetite stirrer. After that, five drops of phenolphthalein, as an acid–base indicator, was added to the mixture and titrated by an HCl solution (0.1 N) up to the equivalent point. After calculation, the the total acidic sites on SO_3H-*L*-His@SiO_2-nano Fe_3O_4 were 0.045 equiv/g of the catalyst and the pH value of 1 g was obtained as 0.74.

In the next step, the efficacy of SO_3H-*L*-His@SiO_2-nano Fe_3O_4 was examined for the synthesis of 3-(1-(2-(1*H*-indol-3-yl)ethyl)-2-aryl-6,6-dimethyl-4-oxo-4,5,6,7-tetrahydro-1*H*-indol-3-yl)indolin-2-ones. In order to optimize the reaction condition, the reaction between 3-phenacylideneoxindole **1a**, triptamine **2,** and dimedone **3**, in 0.5:1:1 molar ratio was considered as a model reaction (Table 1).

In order to determine the influence of the sonication power on the reaction progress, the model reaction was performed in the presence of 40, 60, and 75 W/cm^2 waves

of the apparatus (entries 1–3). The best results were obtained in 60 W/cm^2, and increasing the power up to 75 W/cm^2 did not change the situation notably. The effect of solvents was also examined (entries 4–7). The results confirmed that CH_3CN was the best choice. The catalyst amount was investigated as another parameter. Utilization of 0.02 g of SO_3H-*L*-His@SiO_2-nano Fe_3O_4 under the same reaction conditions revealed that 0.028 was better (compare entries 8 and 2). In order to clarify the critical role of sonic waves in promoting the reaction, the model reaction was carried out in the absence of ultrasound at room temperature and also in refluxing CH_3CN. The results were not satisfactory. This established that the presence of ultrasonic waves was necessary for the reaction to progress (entries 9 and 10). All the reactions were performed in a one-step, one-pot manner.

After optimizing the reaction condition, the reactions between different 3-phenacylideneoxindoles **1a–h**, triptamine **2**, and dimedone **3** were examined in acetonitrile in the presence of 0.028 g of the nanocatalyst under ultrasonic irradiation with power 60 W/cm^2 to obtain the desired products **4a–h**. As can be seen (Table 2), the adducts were obtained within 15–40 min in 71–81% yield. In order to clarify the effect of ultrasonic waves in promoting the reaction, the preparation of **4a** was also carried out in the presence of SO_3H-*L*-His@SiO_2-nano Fe_3O_4 (0.028 g) in CH_3CN a room temperature. The corresponding product was obtained in less than 20% yield within 120 min. This model reaction was carried out in refluxing acetonitrile, but the time was more than when using sonic waves (120 min). This proved the key role of sonication in the synthesis of **6a**, which is due to hot spot theory.

Although the real route for this MCR is not obvious, a proposed mechanism for the synthesis of 3-(1-(2-(1*H*-indol-3-yl)ethyl)-2-aryl-6,6-dimethyl-4-oxo-4,5,6,7-tetrahydro-1*H*-indol-3-yl)indolin-2-ones is illustrated in

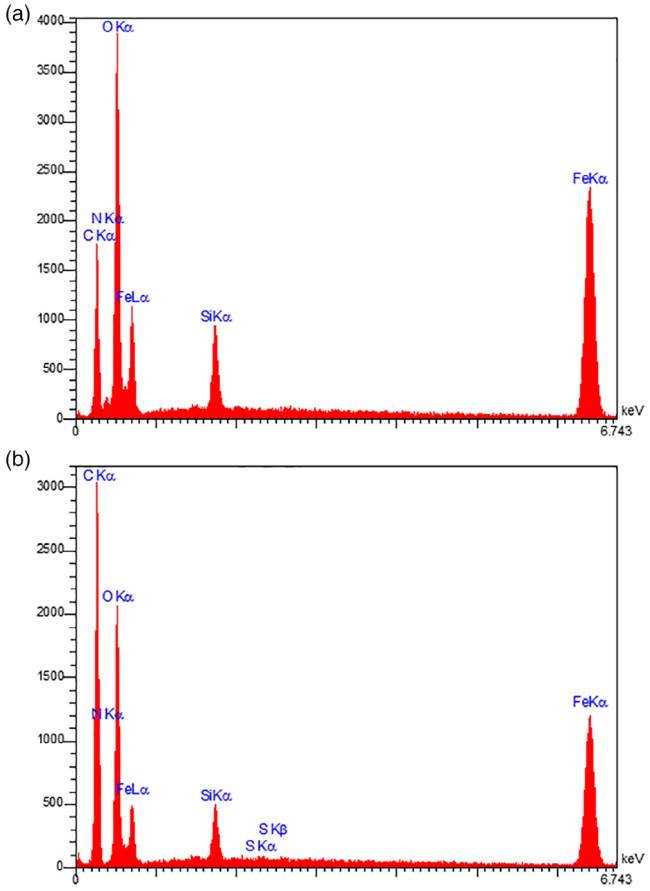

FIGURE 4 EDAX spectrum of the (a) *L*-His@SiO_2-nano Fe_3O_4 and (b) SO_3H-*L*-His@SiO_2-nano Fe_3O_4

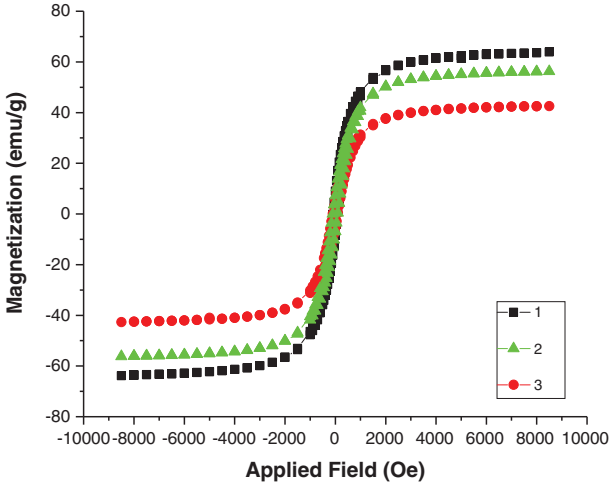

FIGURE 6 VSM curve of (1) commercial nano Fe_3O_4, (2) *L*-His@SiO_2-nano Fe_3O_4, and (3) SO_3H-*L*-His@SiO_2-nano Fe_3O_4

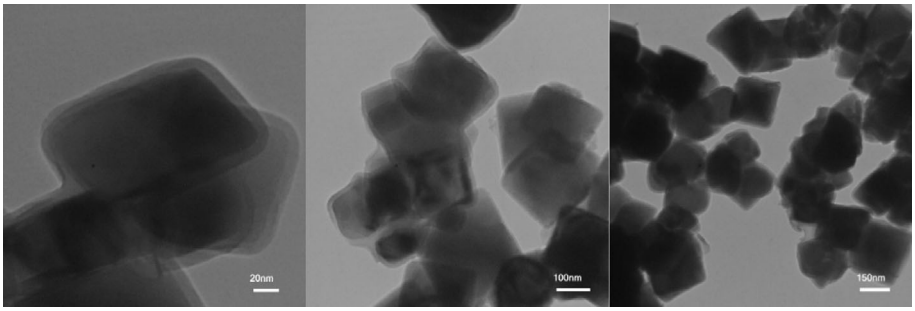

FIGURE 5 TEM images of SO_3H-*L*-His@SiO_2-nano Fe_3O_4

Scheme 3. First, the attack of tryptamine **2** to the activated carbonyl group of dimedone **3**, followed by dehydration, formed the *β*-enaminone **A** intermediate. Then, nucleophilic attack of **A** on 3-phenacylideneoxindole **1** gave the intermediate **B.** Intramolecular cyclization followed by water release gave the desired products **4**.

Recyclability and reusability of catalyst is an important feature in any synthetic methodology. In order to examine this property, preparation of **4a** under ultrasound irradiation was done in the presence SO_3H-*L*-His@nano Fe_3O_4-SiO_2 in CH_3CN. After completion, the catalyst was separated with an external magnet, washed with methanol (3 × 5 mL), and air-dried. The recovered nanocatalyst was used in two more runs of **4a** synthesis successfully (Table 3).

3 | EXPERIMENTAL

3.1 | Materials and apparatus

All materials and solvents were purchased form Aldrich, Merck, or Alfa-Aesar and used without further purification. Commercial nano-magnetite (average particle size of 40–60 nm, purity of 98%) was obtained from Nanosav Co. The FT-IR spectra were recorded from KBr disks by a Bruker FT-IR infrared spectrometer (Transor 27). Melting points were determined by an Electrothermal 9200 instrument and are uncorrected. ^{1}H NMR spectra were recorded with a Bruker drx (300 MHz) machine in DMSO-d_6 solvent. A field-emission scanning electron microscope (FESEM, VEGA\\TESCAN-LMU) was used for measuring the size and morphology of the nanostructures. Mass spectra were obtained by a Gc-Mass 5973 network mass-selective detector on a Gc 6690 Agilent device. EDAX was carried out by a VEGA3 TESCAN machine. TEM images were recorded with a Philips (model MC30) instrument at an accelerating voltage of 300 kV. Magnetization measurements were carried out on a MKTFD VSM. A centrifuge (UNIVERSAL 320) operating at 5000–10,000 rpm was used for the preparation of the nanocatalyst. TGA was recorded by a TGA1 METTLER TOLEDO instrument. Homogenization of the nanostructure was performed in a Wise clean bath with a power of 90 W. The ultrasonic device was an HD 3100 ultrasonic homogenizer (Bandelin Co., Germany). A standard horn SH 70 G emitting 20 kHz ± 500 Hz ultrasound at intensity levels tunable up to a maximum sonic power density of 100 W/cm was used. Sonication was carried out at 100% (maximum amplitude 245 μm). An MS73 probe of 3 mm diameter was immersed directly into the reaction mixture.

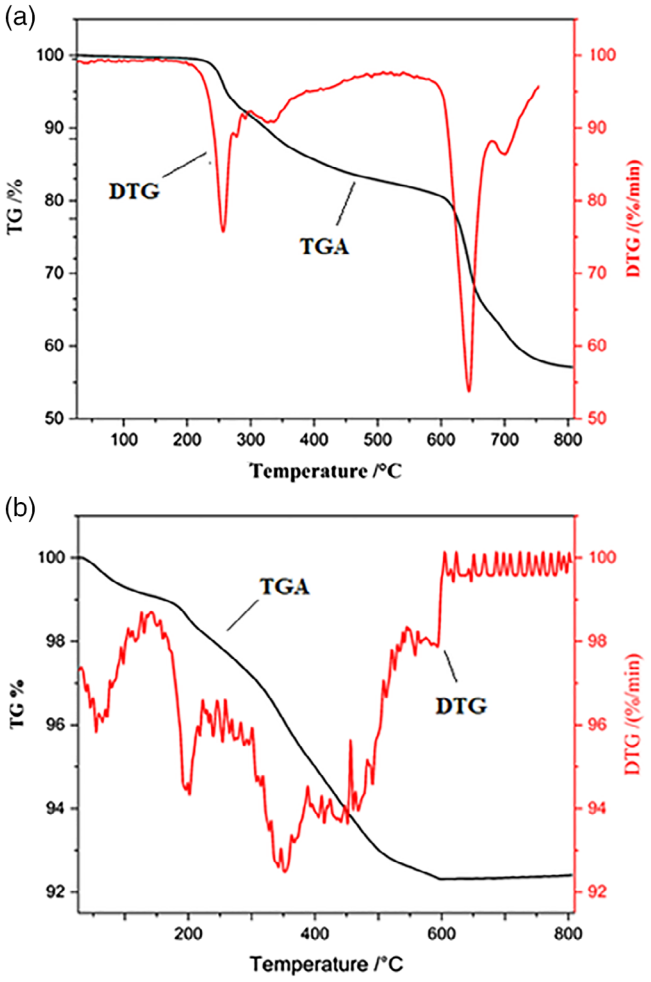

FIGURE 7 TGA/DTG curve of (a) *L*-His@SiO_2-nano Fe_3O_4 and (b) SO_3H-*L*-His@SiO_2-nano Fe_3O_4

3.2 | Catalyst preparation

3.2.1 | Preparation of *L*-His@ SiO_2-nano Fe_3O_4

A mixture of nano Fe_3O_4 (1 g), distilled water (20 mL), absolute ethanol (60 mL), and ammonia (25%, 2 ml) was stirred at room temperature for 10 min and placed in the ultrasound bath for 30 min. Then a mixture of tetraethyl orthosilicate (0.5 mL) in absolute ethanol (1 mL) was added to it dropwise and stirred for 20 h at room temperature. Subsequently, an external magnet was used to collect the solid form the mixture, which was washed further with absolute ethanol (3 × 5 ml). The obtained solid was dried in oven at 70 °C for 5 h. After that, a suspension of *L*-histidine (0.5 g) in diethyl ether (10 mL) was added to the dried solid and stirred for 2 h. Then chloroform (10 mL) was added to the mixture and filtered. The filtrate was washed with chloroform (2 × 10 mL). The obtained solid was air-dried for 1 h and dried at 50 °C for 2 h. The black powder obtained was *L*-His@SiO_2-nano Fe_3O_4 (Scheme 2).

TABLE 1 Optimization the reaction conditions in the ultrasound-assisted synthesis of 3-(1-(2-(1*H*-indol-3-yl)ethyl)-6,6-dimethyl-4-oxo-2-phenyl-4,5,6,7-tetrahydro-1*H*-indol-3-yl)indolin-2-one **4a**[a]

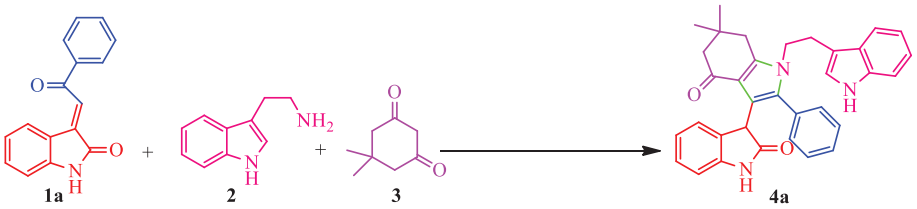

Entry	Conditions			
	Solvent (5 mL)/SO_3H-*L*-His@SiO_2-nano Fe_3O_4 (g)	Ultrasound power (W/cm^2)	Time (min)	Yield[b] (%)
1	CH_3CN/0.028	40	45	70
2	CH_3CN/0.028	60	30	77
3	CH_3CN/0.028	75	30	75
4	EtOAc/0.028	60	60	70
5	EtOH/0.028	60	60	70
6	H_2O/0.028	60	60	20
7	DMSO/0.028	60	60	33
8	CH_3CN/0.02	60	30	55
9[c]	CH_3CN/0.028	—	120	—
10[d]	CH_3CN/0.028	—	140	72

[a]Phenacylideneoxindole (0.5 mmol), triptamine (1 mmol),dimedone (1 mmol).
[b]Isolated yield.
[c]In the absence of sonic waves at room temperature.
[d]In the absence of sonic waves under reflux conditions.

3.2.2 | Preparation of SO_3H-*L*-his@SiO_2-nano Fe_3O_4

A mixture of the obtained *L*-His@SiO_2-nano Fe_3O_4 from the previous section (1 g) in *n*-hexane (10 ml) was sonicated in a bath for 30 min. Then the suspension was poured into a two-necked flask in an ice-bath, and a mixture of chlorosulfonic acid (0.5 g) in *n*-hexane (10 mL) in a drop-funnel was added dropwise to the flask while mixing. The stirring was continued for 30 min in order to remove the HCl gas form the flask. Subsequently, methanol (10 mL) added to the mixture and stirred at room temperature for 45 min. Filtrating the mixture followed by washing the solid with *n*-hexane (10 mL) and distilled water (20 mL) gave a black solid, which was dried at 60 °C in an oven for 4 h, resulting in SO_3H-*L*-His@SiO_2-nano Fe_3O_4 (Scheme 2).

3.3 | General procedure for the synthesis of 3-phenacylideneoxindoles 1a–h

The substrates, 3-phenacylideneoxindoles, were synthesized according to the previously procedure.[36] A mixture of isatins (20 mmol) and acetophenone derivatives (20 mmol) in the presence of dimethylamine (20 mmol) was stirred for 5 min. Then acetic acid (20 mL) and HCl (37%, 20 mL) were added and refluxed at 78 °C for 30 min. The progress of the reaction was monitored by TLC (eluent, *n*-hexane/EtOAc, 1:1). The reaction mixture was extracted with equal amounts of water and EtOAc. Evaporating the solvent and crystallization from absolute ethanol gave the corresponding 3-phenacylideneoxindoles **1a–h** as colored powders (orange, red, brown) in 71–97% yield.

3.4 | General procedure for the synthesis of 3-(1-(2-(1*H*-indol-3-yl)ethyl)-2-aryl-6,6-dimethyl-4-oxo-4,5,6,7-tetrahydro-1*H*-indol-3-yl)indolin-2-ones 4a–h

A mixture 3-phenacylideneoxindoles **1a–h** (0.5 mmol), tryptamine **2** (1 mmol), and dimedone **3** (1 mmol) in the presence of SO_3H-*L*-His@SiO_2-nano Fe_3O_4 (0.028 g) in CH_3CN (20 mL) was irradiated with ultrasonic waves (60 W/cm^2(for an appropriate time as monitored by TLC (eluent, *n*-hexane/EtOAc, 1:1). After completion of the reaction, the reaction mixture was dissolved in methanol

TABLE 2 Ultrasound-assisted synthesis of 3-(1-(2-(1*H*-indol-3-yl)ethyl)-2-aryl-6,6-dimethyl-4-oxo-4,5,6,7-tetrahydro-1*H*-indol-3-yl) indolin-2-ones **4a–h** by SO_3H-*L*-His@SiO_2-nano Fe_3O_4 in CH_3CN at room temperature[a]

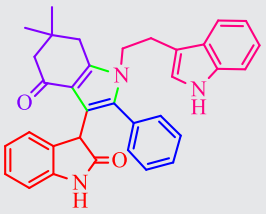

4a
25 min, 77%[b]
101–104°C

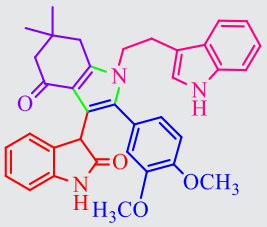

4b
25 min, 81%
66–68°C

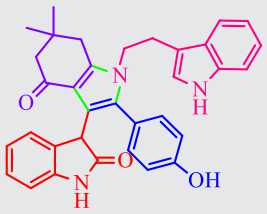

4c
15 min, 80%
67–70°C

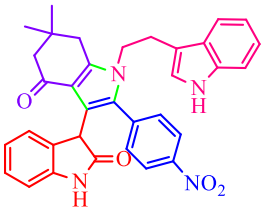

4d
20 min, 76%
73–76°C

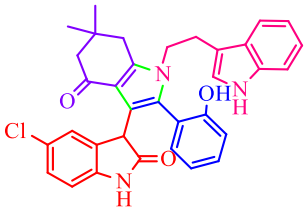

4e
40 min, 71%
80–83°C

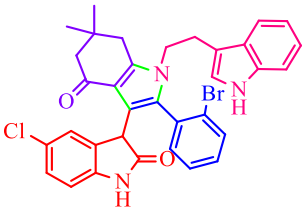

4f
20 min, 73%
85–87°C

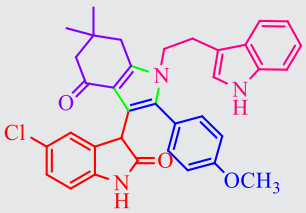

4g
35 min, 74%
67–70°C

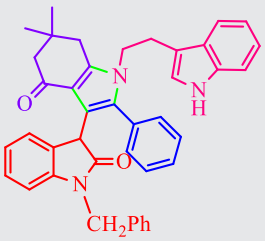

4h
20 min, 71%
68–71°C

[a]3-Phenacylideneoxindoles **1a–h** (0.5 mmol), triptamine **2** (1 mmol), dimedone **3** (1 mmol), and SO_3H-*L*-His@SiO_2-nano Fe_3O_4 (0.028 g).
[b]Isolated yields.

(20 mL) and the catalyst separated by an external magnet (0.7 T). The pure products **4a–h** were obtained from the crude mixture through plate chromatography in 71–81% yield (Table 2).

3.4.1 | 3-(1-(2-(1*H*-indol-3-yl)ethyl)-6,6-dimethyl-4-oxo-2-phenyl-4,5,6,7-tetrahydro-1*H*-indol-3-yl)indolin-2-one (4a)

Dark yellow powder; m.p.: 101–104°C. FT-IR (KBr) ν (cm^{-1}): 3248, 3057, 2955, 2927, 2869, 1706, 1538, 1461, 1271, 1151, 1367, 812, 742, 610. ^{1}H NMR (300 MHz, DMSO-d_6): δ (ppm) 0.95 (s, 6H, 2Me), 1.96–2.17 (m, 4H, $2CH_2$), 2.91 (m, 2H, CH_2), 3.09–3.26 (m, 2H, CH_2), 4.88 (s, 1H, CH), 6.82–7.17 (m, 7H, Ar), 7.32–7.34 (m, 3H, Ar), 7.48–7.50 (m, 4H, Ar), 10.26 (s, 1H, NH), 10.87 (s, 1H, NH). ^{13}C NMR (75 MHz, DMSO-d_6): δ (ppm) 23.68, 28.21, 32.20, 42.11, 43.01, 50.33, 93.25, 111.43, 118.28, 120.91, 122.81, 127.13, 136.20, 162.72, 193.85. MS (ESI) *m/z* 513 [M^+], 485 [M^+] – $2CH_3$, 461 [M^+]—$C(CH_3)_2$, —CO, 429 [M^+]—$C(CH_3)_4$, —CO, 403 [M^+]—$C(CH_3)_4$, —CO, —CH_2CH_2, 280 [M^+]—CH_2CH_2, —2Me, —indolyl, 254 [M^+]—CH_2, —CMe_2, —indolyl, 212 [M^+]—$CH_2CMe_2CH_2$, —indolyl, —CO, 130 (oxindolyl), 67 (pyrolyl).

3.4.2 | 3-(1-(2-(1H-indol-3-yl)ethyl)-2-(3,4-dimethoxyphenyl)-6,6-dimethyl-4-oxo-4,5,6,7-tetrahydro-1H-indol-3-yl) indolin-2-one (4b)

Lemon powder; mp: 66–68°C. FT-IR (KBr) ν (cm^{-1}): 3,385, 3,256, 3,058, 2,954, 2,926, 1,513, 1,460, 1,382, 1,269, 1,150, 1,100, 811, 742. ^{1}H NMR (300 MHz, DMSO-d_6): δ (ppm) 0.96 (s, 6H, 2Me), 1.96 (s, 3H, OMe), 2.17 (s, 3H, OMe), 2.49 (s, 1H, CH_2), 2.52 (s, 1H, CH_2), 2.89–2.95 (m, 1H, CH_2), 3.26–3.35 (m, 3H, CH_2), 4.89 (s, 1H, CH), 6.44–6.99 (m, 2H, Ar), 7.03–7.06 (m, 4H, Ar), 7.08 (s, 1H, Ar), 7.18 (s, 1H, Ar), 7.32–7.35 (m, 2H, Ar), 7.48–7.51 (m, 2H, Ar), 10.52 (s, 1H, NH), 10.87 (s, 1H, NH). ^{13}C NMR (75 MHz, DMSO-d_6): δ (ppm) 23.65, 27.98, 32.19, 42.10, 42.97, 50.32, 93.22, 111.39, 111.44, 118.07, 118.27, 120.91, 122.85, 127.11, 136.19, 162.57, 193.75. MS (ESI) *m/z* 573 [M^+], 503 [M^+ – $2CH_2$ – CMe_2], 429 [M^+ – $2CH_2$ – CMe_2 – MeO – CO – NH], 405 [M^+ – $C_6H_4(OMe)_2$ – 2Me], 323 [M^+ – $C_6H_4(OMe)_2$ – indolyl], 298 [M^+– indolyl – oxindolyl – $2CH_2$], 282 [M^+ – $C_6H_4(OMe)_2$ – indolyl –$2CH_2$], 267 [M^+– $C_6H_4(OMe)_2$ – indolyl – $2CH_2$ –Me], 223 [M^+ – $C_6H_4(OMe)_2$ – indolyl – $2CH_2$ – 2Me – CO], 138 ($C_6H_4(OMe_3)_2$), 130 (oxindolyl), 117 (indolyl).

3.4.3 | 3-(1-(2-(1*H*-indol-3-yl)ethyl)-2-(4-hydroxyphenyl)-6,6-dimethyl-4-oxo-4,5,6,7-tetrahydro-1*H*-indol-3-yl)indolin-2-one (4c)

Brownish red powder; m.p.: 67–70 °C. FT-IR (KBr) ν (cm^{-1}): 3675, 3394, 3061, 2924, 2855, 1680, 1605, 1510, 1461, 1377, 1228, 1184, 742. ^{1}H NMR (300 MHz, DMSO-d_6): δ (ppm) 0.92 (s, 6H, 2Me), 2.49–2.52 (m, 2H, CH_2), 2.97–3.02 (m, 2H, CH_2), 3.03–3.07 (m, 2H, CH_2), 3.34–3.49 (m, 2H, CH_2), 3.50 (s, 1H, CH), 6.82–7.11 (m, 6H, Ar, OH), 7.23–7.31 (m, 1H, Ar), 7.50–7.52 (m, 2H, Ar), 7.52–7.85 (m, 1H, Ar), 7.83–8.13 (m, 2H, Ar), 8.50–8.53 (m, 1H, Ar), 10.84 (s, 1H, NH), 12.14 (s, 1H, NH).

3.4.4 | 3-(1-(2-(1*H*-indol-3-yl)ethyl)-6,6-dimethyl-2-(4-nitrophenyl)-4-oxo-4,5,6,7-tetrahydro-1*H*-indol-3-yl)indolin-2-one (4d)

Brownish orange powder; m.p.: 73–76°C. IR (KBr) ν (cm^{-1}): 3383, 3249, 3057, 2954, 2926, 2867, 1531, 1457, 1383, 1270, 1366, 1189, 1151, 741. ^{1}H NMR (300 MHz, DMSO-d_6): δ (ppm) 0.96 (s, 6H, $2CH_3$), 1.99–2.19 (m, 4H, $2CH_2$), 2.94–3.11 (m, 2H, CH_2), 2.95–3.28 (m, 2H, CH_2), 4.94 (s, 1H, CH), 6.98–7.18 (m, 8H, Ar), 7.35–7.50 (m, 5H, Ar), 10.28 (s, 1H, NH), 10.93 (s, 1H, NH). ^{13}C NMR (300 MHz, DMSO-d_6): δ (ppm) 23.71, 28.02, 32.23, 42.15, 43.06, 50.33, 93.25, 111.47, 118.14, 118.32, 120.95, 122.90, 127.15, 136.25, 162.81, 193.96.

3.4.5 | 3-(1-(2-(1*H*-indol-3-yl)ethyl)-2-(2-hydroxyphenyl)-6,6-dimethyl-4-oxo-4,5,6,7-tetrahydro-1H-indol-3-yl)-5-chloroindolin-2-one (4e)

Light brownish orange powder; m.p.: 80–83 °C. IR (KBr) ν (cm^{-1}): 3649, 3419, 2925, 2854, 1715, 1634, 1592, 1456, 1523, 1199, 1155, 1283, 596, 744. ^{1}H NMR (300 MHz, DMSO-d_6): δ (ppm) 0.95 (s, 6H, $2CH_3$), 1.84 (m, 2H, CH_2), 1.95 (m, 2H, CH_2), 2.17 (m, 2H, CH_2), 2.91–2.93 (m, 2H, CH_2), 4.87 (s, 1H, CH), 6.77–6.79 (m, 1H, Ar), 6.82–6.88 (m, 1H, Ar), 6.91–6.99 (m, 2H, Ar), 7.02–7.05 (m, 3H, Ar), 7.17–7.32 (m, 3H, Ar), 7.48–7.50 (m, 2H, Ar), 7.65 (brs, 1H, OH), 10.48 (brs, 1H, NH), 10.91 (brs, 1H, NH). MS (ESI) *m/z* 503 [M^+ – $2CH_2$ – Cl], 451 [M^+ – Cl – C_6H_5], 435 [M^+ – C_6H_4OH – Cl], 420 [M^+ – C_6H_4OH – Cl – Me], 365 [M^+ – C_6H_4OH – Cl – Me – $CH_2CMe_2CH_2$], 365 [M^+ C_6–H_4OH – Cl – Me – $CH_2CMe_2CH_2$ – CO], 168 (5-cloxindolyl), 130 (oxindolyl), 117 (indolyl).

3.4.6 | 3-(1-(2-(1*H*-indol-3-yl)ethyl)-2-(2-bromophenyl)-6,6-dimethyl-4-oxo-4,5,6,7-tetrahydro-1*H*-indol-3-yl)-5-chloroindolin-2-one (4f)

Dark brownish orange powder; m.p.: 85–87°C. IR (KBr) ν (cm^{-1}): 3422, 2925, 2855, 1647, 1560, 1457, 1384, 1269, 1115, 695, 743. ^{1}H NMR (300 MHz, DMSO-d_6): δ (ppm) 0.95 (s, 6H, $2CH_3$), 1.21 (m, 1H, CH), 1.79–1.95 (m, 2H, CH_2), 2.17 (m, 2H, CH_2), 2.48–2.52 (m, 1H, CH), 2.91–2.93 (m, 2H, CH2), 4.87 (s, 1H, CH), 6.94–6.99 (m, 2H, Ar), 7.02–7.07 (m, 3H, Ar), 7.13–7.17 (m, 3H, Ar), 7.33 (d, J = 7.82 Hz, 2H, Ar), 7.49 (d, J = 7.48 Hz, 2H, Ar), 10.25 (s, 1H, NH), 10.91 (s, 1H, NH). MS (ESI) *m/z* 553 [M^+ – $C(Me)_4$], 491 [M^+ – $C(Me)_4$ – CO – Cl], 413 [M^+ – $C(Me)_4$ – CO – Cl – Br], 387 [M^+ – $C(Me)_2CH_2CH_2$ – CO – $(CH_2)_2$ – indolyl], 323 [M^+ – $C(Me)_2$ – $(CH_2)_2$ – indolyl –Br –Cl], 182 (3-Me-5-cloxindolyl), 130 (oxindolyl).

3.4.7 | 3-(1-(2-(1*H*-indol-3-yl)ethyl)-2-(4-methoxyphenyl)-6,6-dimethyl-4-oxo-4,5,6,7-Tetrahydro-1*H*-indol-3-yl)-5-chloroindolin-2-one (4g)

Yellow crystal; m.p.: 67–70°C. IR (KBr) ν (cm^{-1}); 3384, 3249, 3057, 2954, 2925, 2867, 1536, 1458, 1366, 1150, 1270,

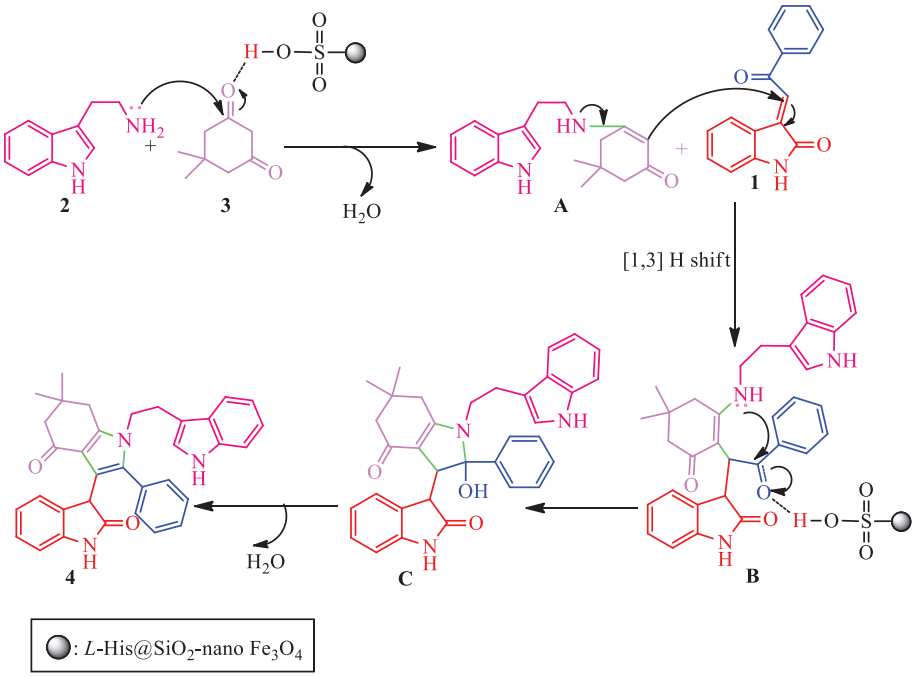

SCHEME 3 Proposed mechanism for the sonosynthesis of **4**

TABLE 3 Recyclability of SO_3H-*L*-His@nano Fe_3O_4-SiO_2 in sono-synthesis of **4a**

No. of cycle	Time (min)	Yield (%)
1	25	77
2	25	75
3	25	73

741, 873. ^{1}H NMR (300 MHz, DMSO-d_6): δ (ppm) 0.96 (m, 6H, $2CH_3$), 1.98 (m, 2H, CH_2), 2.18 (m, 2H, CH_2), 2.93 (m, 2H, CH_2), 3.27 (m, 5H, CH_2, OMe), 4.91 (s, 1H, CH), 6.98 (d, J = 6.35 Hz, 2H, Ar), 7.06–7.09 (m, 5H, Ar), 7.18 (m, 1H, Ar), 10.35 (s, 1H, NH), 10.90 (s, 1H, NH). ^{13}C NMR (75 MHz, DMSO-d_6): δ(ppm) 23.67, 27.48, 32.19, 42.11, 42.98, 50.33, 93.23, 111.44, 118.07, 118.27, 120.41, 122.86, 127.12, 136.21, 162.65, 193.80. MS (ESI) *m/z* 505 [M^+ – CO – $C(Me)_2CH_2CH_2$], 432 [M^+ – indolyl – CH_2CH_2], 402 [M^+ – indolyl – CH_2CH_2 – 2Me], 384 [M^+– indolyl –CH_2CH_2 – 3Me – Cl], 327 [M^+– indolyl – CH_2CH_2 – Cl – $C(Me)_2CH_2CH_2$], 282 [M^+ – 5-cloxindolyl – indolyl – Me], 267 [M^+ – 5-cloxindolyl – indolyl – Me – CH_2CH_2], 182 (3-Me-5-cloxindolyl), 130 (oxindolyl).

3.4.8 | 3-(1-(2-(1*H*-indol-3-yl)ethyl)-6,6-dimethyl-4-oxo-2-phenyl-4,5,6,7-tetrahydro-1*H*-indol-3-yl)-1-benzylindolin-2-one (4h)

Mustardy powder; m.p.: 68–71 °C. IR (KBr) ν (cm^{-1}); 3384, 3250, 3057, 2954, 2925, 2859, 1537, 1459, 1381, 1270, 1150, 1100, 741, 611. ^{1}H NMR (300 MHz, DMSO-d_6): δ (ppm) 0.96 (m, 6H, $2CH_3$), 1.97 (m, 2H, CH_2), 2.17 (m, 2H, CH_2), 2.48–2.52 (m, 2H, CH_2), 2.90–2.94 (m, 2H, CH_2), 3.24–3.28 (m, 2H, CH_2), 4.90 (s, 1H, CH), 6.95–6.99 (m, 2H, Ar), 7.03–7.10 (m, 6H, Ar), 7.18 (m, 2H, Ar), 7.34 (d, J = 7.95 Hz, 2H, Ar), 7.50 (d, J = 7.70 Hz, 2H, Ar), 10.89 (s, 1H, NH). ^{13}C NMR (75 MHz, DMSO-d_6): δ (ppm) 23.66, 28, 32.21, 42.10, 42.99, 50.23, 93.23, 111.42, 111.45, 118.09, 118.27, 120.92, 122.87, 127.12, 136.20, 162.62, 193.79. MS (ESI) *m/z* 504 [M^+ – CO – $C(Me)_2CH_2CH_2$], 479 [M^+ – benzyl – 2Me], 401 [M^+ – benzyl – CH_2CH_2 – CMe_2], 282 [M^+ –$CMe_2CH_2CH_2$ – indolyl – phenyl – CO – CH_2CH_2], 267 [M^+ – benzyloxindolyl – indolyl], 252 [M^+ – benzyloxindolyl – indolyl – Me], 225 (N-benzyloxindolyl), 130 (oxindolyl).

4 | CONCLUSIONS

In summary, a novel and simple procedure for the sonosynthesis of 3-(1-(2-(1*H*-indol-3-yl)ethyl)-2-aryl-6,-6-dimethyl-4-oxo-4,5,6,7-tetrahydro-1*H*-indol-3-yl)indolin-2-ones through a three-component reaction of tryptamine, dimedone, and 3-phenacylideneoxindoles by a novel core-shell nanocatalyst anchoring sulfonated *L*-histidine on magnetized silica (SO_3H-*L*-His@SiO_2-nano Fe_3O_4) is reported for the first time. This procedure has several advantages, such as utilizing a bio-based nanocatalyt in the synthesis of some valuable heterocycles, performing the reaction in the presence of ultrasound irradiation as a powerful and green technique, separating the SO_3H-*L*-His@SiO_2-nano Fe_3O_4 with an external magnet, recoverability of the catalyst as a

green aspect of the method, to obtain the desired products as novel substances.

ACKNOWLEDGMENTS

This work was supported by Alzahra University.

ORCID

Kobra Nikoofar https://orcid.org/0000-0002-3950-8229

REFERENCES

[1] A. Leoni, A. Locatelli, R. Morigi, M. Rambaldi, *Expert Opin. Ther. Pat.* **2016**, *26*, 149.
[2] I. G. Salado, J. Zaldivar-Diez, V. Sebastian, L. Li, L. Geiger, S. Gonzalez, N. E. Campillo, C. Gil, A. V. Morales, D. I. Perez, A. Martinez, *Eur. J. Med. Chem.* **2017**, *138*, 328.
[3] T. Tokunaga, W. E. Hume, T. Umezome, K. Okazaki, Y. Ueki, K. Kumagai, S. Hourai, J. Nagamine, H. Seki, M. Taiji, H. Noguchi, R. Nagata, *J. Med. Chem.* **2001**, *44*, 4641.
[4] A. L. Cheryl, B. M. Phyllis, L. W. F. Stacey, F. B. Joseph, W. R. Anthony, M. P. Rosenberg, C. J. Henry, K. L. Mitchener, M. K. Klein, J. G. Hintermeister, P. J. Bergman, G. C. Couto, G. N. Mauldin, G. M. Michels, *Clin. Cancer Res.* **2009**, *15*, 3856.
[5] C. R. Prakash, P. Theivendren, S. Raja, *Pharmacol. Pharm.* **2012**, *3*, 62.
[6] S. P. Singh, K. Jha, *Zentralbl. Mikrobiol.* **1989**, *144*, 105.
[7] R. K. Thakur, P. Joshi, P. Baranwal, G. Sharma, S. K. Shukla, R. Tripathi, R. P. Tripathi, *Eur. J. Med. Chem.* **2018**, *155*, 764.
[8] R. Meleddu, S. Distinto, A. Corona, G. Bianco, V. Cannas, F. Esposito, A. Artese, S. Alcaro, P. Matyus, D. Bogdan, F. Cottiglia, E. Tramontano, E. Maccioni, *Eur. J. Med. Chem.* **2015**, *93*, 452.
[9] R. Dalpozzo, G. Bartoli, G. Bencivenni, *Chem. Soc. Rev.* **2012**, *41*, 7247.
[10] A. Perry, R. J. K. Taylor, *Chem. Commun.* **2009**, *2009*,3249.
[11] G. M. Ziarani, R. Moradi, N. Lashgari, *Tetrahedron* **2018**, *74*, 1323.
[12] R. Dalpozzo, *Adv. Synth. Catal.* **2017**, *359*, 1772.
[13] G. Mohammadi Ziarani, P. Gholamzadeh, N. Lashgari, P. Hajiabbasi, *ARKIVOC* **2013**, *i*, 470.
[14] G. Cravotto, P. Cintas, *Chem. Soc. Rev.* **2006**, *35*, 180.
[15] B. Banerjee, *Ultrason. Sonochem.* **2017**, *35*, 15.
[16] P. Cintas, *Ultrason. Sonochem.* **2016**, *28*, 257.
[17] N. A. Khan, S. H. Jhung, *Coord. Chem. Rev.* **2015**, *285*, 11.
[18] H. Xu, B. W. Zeiger, K. S. Suslick, *Chem. Soc. Rev.* **2013**, *42*, 2553.
[19] C. Su, *J. Hazard. Mater.* **2017**, *322*, 48.
[20] L. Mohammed, H. G. Gomaa, D. Ragab, *Particuology* **2017**, *30*, 1.
[21] O. A. Inozemtseva, S. V. German, N. A. Navolokin, A. B. Bucharskaya, G. N. Maslyakova, D. A. Gorin, *Nanotechnol. Biosensors Adv. Nanomater.* **2018**, *2018*, 175.
[22] R. A. Revia, M. Zhang, *Mater. Today* **2016**, *19*, 157.
[23] S. V. German, N. A. Navolokin, N. R. Kuznetsova, V. V. Zuev, O. A. Inozemtseva, A. A. Anis'kov, E. K. Volkova, A. B. Bucharskaya, G. N. Maslyakova, R. F. Fakhrullin, G. S. Terentyuk, E. L. Vodovozova, D. A. Gorin, *Colloids Surf. B Biointerfaces* **2015**, *135*, 109.
[24] M. F. Zawrah, E. S. E. El Shereefy, A. Y. Khudir, *Silicon* **2019**, *11*, 85.
[25] M. B. Gawande, P. S. Branco, R. S. Varma, *Chem. Soc. Rev.* **2013**, *42*, 3371.
[26] L. Hadian-Dehkordi, H. Hosseini-Monfared, *Green Chem.* **2016**, *18*, 497.
[27] A. Baeza, G. Guillena, D. J. Ramón, *ChemCatChem* **2016**, *8*, 49.
[28] M. Esmaeilpour, A. R. Sardarian, H. Firouzabadi, *ChemistrySelect* **2018**, *3*, 9236.
[29] E. Pourian, S. Javanshir, Z. Dolatkhah, S. Molaei, A. Maleki, *ACS Omega* **2018**, *3*, 5012.
[30] K. Nikoofar, F. Mehrikaram, *Polyhedron* **2019**, *159*, 330.
[31] K. Nikoofar, F. Molaei Yielzoleh, *Res. Chem. Intermed.* **2018**, *44*, 7353.
[32] K. Nikoofar, H. Heidari, Y. Shahedi, *Cellul.* **2018**, *25*, 5697.
[33] K. Nikoofar, S. Khani, *Catal. Lett.* **2018**, *148*, 1651.
[34] K. Nikoofar, Z. Khademi, M. Haghighi, *J. Chem. Sci.* **2016**, *128*, 1805.
[35] Y.-H. Jiang, G. G. Yan, *Synthesis* **2016**, *48*, 3057.
[36] J. Azizian, M. Shaabanzadeh, F. Hatamjafari, M. R. Mohammadizadeh, *ARKIVOC* **2006**, *xi*, 47.

SUPPORTING INFORMATION

Additional supporting information may be found online in the Supporting Information section at the end of this article.

How to cite this article: Nikoofar K, Peyrovebaghi SS. Ultrasound-assisted synthesis of 3-(1-(2-(1*H*-indol-3-yl)ethyl)-2-aryl-6,6-dimethyl-4-oxo-4,5,6,7-tetrahydro-1*H*-indol-3-yl)indolin-2-ones by novel core-shell bio-based nanocatalyst anchoring sulfonated *L*-histidine on magnetized silica (SO_3H-*L*-His@SiO_2-nano Fe_3O_4). *J Chin Chem Soc*. 2020;1–11. https://doi.org/10.1002/jccs.201900365